# Local magnetic response of superconducting $Sr_2RuO_4$ thin films

G. M. Ferguson,[1,*] Hari P. Nair,[2] Nathaniel J. Schreiber,[2] Ludi Miao,[1,3] Kyle M. Shen,[1,4] Darrell G. Schlom,[2,4,5] and Katja C. Nowack[1,4,†]

[1]*Department of Physics, Laboratory of Atomic and Solid State Physics, Cornell University, Ithaca, New York 14853, USA*
[2]*Department of Materials Science and Engineering, Cornell University, Ithaca, New York 14853, USA*
[3]*Department of Physics, New Mexico State University, Las Cruces, New Mexico 88003, USA*
[4]*Kavli Institute at Cornell for Nanoscale Science, Ithaca, New York 14853, USA*
[5]*Leibniz-Institut für Kristallzüchtung, Max-Born-Straße 2, 12489 Berlin, Germany*

(Received 25 March 2024; revised 4 September 2024; accepted 5 September 2024; published 11 October 2024)

We conduct local magnetic measurements on superconducting thin-film samples of $Sr_2RuO_4$ using scanning superconducting quantum interference device (SQUID) susceptometry. From the diamagnetic response, we extract the magnetic penetration depth, $\lambda$, which exhibits a quadratic temperature dependence at low temperatures. In high-purity bulk samples, a similar quadratic temperature dependence has been attributed to nonlocal electrodynamics. Although we cannot exclude nonlocal effects, our analysis indicates that in our thin-film samples the presence of scattering is sufficient to explain the temperature dependence of $\lambda$. While we observe micron-scale variations in the diamagnetic response and superconducting transition temperature, the form of the temperature dependence of $\lambda$ is independent of position. The growth and local characterization of superconducting thin-film $Sr_2RuO_4$ samples demonstrated here is a first step toward device-based tests of the superconducting order parameter in $Sr_2RuO_4$.

DOI: 10.1103/PhysRevB.110.144510

Since the discovery of superconductivity in $Sr_2RuO_4$ [1], a substantial research effort has been dedicated to the determination of the superconducting order parameter [2–6]. Although early experiments were interpreted in favor of an odd-parity, time reversal symmetry breaking order parameter, recent experiments have called this picture into question [7–11]. High-quality superconducting thin films of $Sr_2RuO_4$ have recently been grown by molecular-beam epitaxy [12], raising the prospect of device-based tests of the order parameter symmetry [13]. Given the extreme sensitivity of the superconducting state in $Sr_2RuO_4$ to disorder [14,15] and the presence of new types of defects in $Sr_2RuO_4$ thin films [16–18], a direct comparison between the superconducting properties of thin films and bulk single crystals is needed to set the stage for using thin-film devices to study the order parameter in $Sr_2RuO_4$.

The dependence on temperature, $T$, of the magnetic penetration depth, $\lambda$, contains information about the gap structure of superconductors. A nodal superconducting gap gives rise to a power-law dependence of $\lambda(T)$ at low temperature, while a fully gapped superconductor exhibits an exponential temperature dependence. In $Sr_2RuO_4$, the observation of $\lambda(T) - \lambda_0 \sim T^2$ with $\lambda_0$ the zero-temperature value in high-quality bulk single crystals provided early evidence for the presence of nodes in the superconducting gap function [19].

Here, we study the superconducting penetration depth in a 25 nm thick $Sr_2RuO_4$ thin film grown by molecular-beam epitaxy. The substrate is $(LaAlO_3)_{0.29}$–$(SrAl_{0.5}Ta_{0.5}O_3)_{0.71}$ (LSAT) with the $c$ axis oriented perpendicular to the substrate surface. The LSAT substrate preserves the tetragonal symmetry of $Sr_2RuO_4$ and induces a small tensile strain of approximately 0.045% due to the lattice constant mismatch between LSAT and bulk $Sr_2RuO_4$ when the sample is cooled to low temperatures. In the Supplemental Material [20], we estimate that the small expected change of the critical temperature is minimal based on uniaxial pressure experiments on bulk single crystals [7,21,22]. Quantum oscillation studies on $Sr_2RuO_4$ thin films prepared by the same methods and on the same substrate as ours [16] show that the Fermi surface areas and density of states is the same as in bulk samples. Therefore, the small epitaxial strain is expected to induce negligible changes in the electronic structure and critical temperature of the films. Details of the growth of these films are described in Ref. [12] and in Appendix C. We determine the residual resistance ratio (RRR), here defined as the ratio of the resistances measured at 300 K and 4 K, as RRR = 81 for the film studied here. The resistance measurements are shown in the Supplemental Material [20].

Our experimental approach is illustrated schematically in Fig. 1(a). We use a scanning superconducting quantum interference device (SQUID) susceptometer [23,24] to detect the diamagnetic response of the superconducting film to a local magnetic field produced by a current $I_{FC}$ sourced through an integrated field coil with radius $a$. In the superconducting state, the $Sr_2RuO_4$ film generates supercurrents that screen the magnetic field produced by the field coil, effectively reducing the mutual inductance $M$ between the field coil and the SQUID pickup loop.

*Now at Max Planck Institute for Chemical Physics of Solids.
†Contact author: kcn34@cornell.edu

 

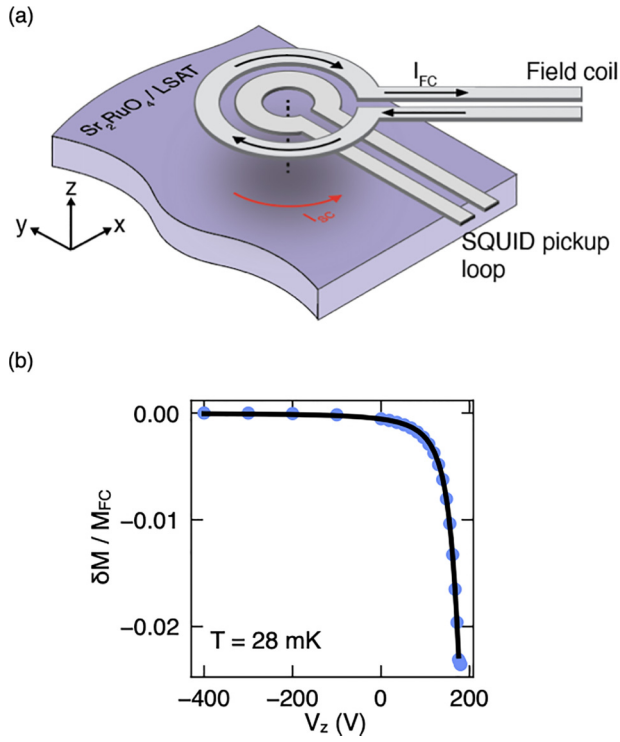


FIG. 1. (a) Schematic of the SQUID pickup loop and field coil pair close to the surface of an $Sr_2RuO_4$ thin film grown on an LSAT substrate. A current $I_{FC}$ applied to the field coil with an inner diameter of 8 μm induces a screening current $I_{SC}$ in the superconducting $Sr_2RuO_4$. The sample response to $I_{FC}$ is detected via the SQUID pickup loop, with an inner diameter of 1.5 μm. (b) Change in mutual inductance $\delta M$ between the SQUID and field coil as the voltage $V_z$ applied to the $z$-positioner is increased, bringing the susceptometer toward the sample surface. The solid line is a fit to Eq. (1).

In Fig. 1(b) we show the change in the measured mutual inductance $\delta M/M_{FC}$ at a fixed temperature, as the susceptometer approaches the sample surface. Here, we set $\delta M = 0$ when the SQUID is far from the sample, and $M_{FC}$ is the bare mutual inductance between the SQUID pickup loop and field coil, which we measured to be 330 $\Phi_0$/A far from the sample surface. With these choices, $\delta M/M_{FC} = -1$ would correspond to a complete screening of the magnetic field in the plane of the pickup loop. The signals that we observe correspond to a fraction of this value as expected for a thin film. In the Pearl limit $\lambda \gg d$ with $d$ the film thickness and neglecting the finite thickness and detailed geometry of the pickup loop and field coil, Kogan and Kirtley *et al.* derived a model for the dependence of $\delta M/M_{FC}$ on the height $z$ above the sample [25,26]:

$$\frac{\delta M(z,T)}{M_{FC}} = -\frac{ad}{2\lambda^2(T)}\left[1 - \frac{2z}{\sqrt{a^2+4z^2}}\right]. \quad (1)$$

In Fig. 1(b) we include a fit to Eq. (1) of the height dependence of $\delta M/M_{FC}$. To determine the height $z$ above the sample in Eq. (1), we use $z = z_0 + \alpha(V_z - V_{z0})$, where $z_0$ and $V_{z0}$ are the height and piezo-positioner voltage when the SQUID chip first makes mechanical contact with the sample. In this case, we identify $V_{z0} = 175$ V as the value of $V_z$ where $\delta M$ becomes only weakly $V_z$ dependent, indicating that the SQUID has made contact with the sample surface. The parameter $\alpha$ determines the change in SQUID height per volt applied to the piezo positioner. To perform the fit in Fig. 1(b), we constrain the geometric parameters in the model, which we can estimate at room temperature, $a = 4$ μm, $d = 25$ nm, and $z_0 = 4$ μm. The estimated value of $z_0$ is based on our alignment and the SQUID geometry. We estimate $a$ using the lithographic dimensions of the field coil. The fitting procedure yields $\lambda = 480$ nm and $\alpha = 120$ nm $V^{-1}$. These values agree reasonably well with previous measurements of $\alpha$ for our scanner and estimates of the low-temperature value of $\lambda$ for films with a $T_c$ of ∼900 mK (see Appendix A for details). The absolute value of $\lambda$ is affected by uncertainty in the model parameters, which are strongly correlated with $\lambda$, making a meaningful determination of the absolute value of $\lambda$ challenging (see Appendix A for details). For example, given the large uncertainty in the geometric parameters $d$, $z_0$, and $a$, we can only constrain $\lambda$ to lie between 210 nm and 860 nm based on the height sweep data in Fig. 1(b). Recent studies on high-quality bulk single crystals with $T_c$ close to 1.5 K reported the absolute value of the low-temperature penetration depth to be between 120 nm and 130 nm [27,28]. Earlier work on bulk samples with a few values of $T_c$ showed that samples with lower $T_c$ have a longer low-temperature penetration depth [29]. Specifically, Ref. [29] estimated $\lambda_0$ to be 300 nm and 410 nm for two samples with $T_c$ of 1.24 K and 0.7 K, respectively. These values are consistent with the value we estimate for our thin film given the large uncertainty in estimating the absolute value of $\lambda$ from our data.

An important feature of Eq. (1) is that its sole temperature dependence originates from $\lambda(T)$, which appears in a simple prefactor. This implies that by measuring $M$ as a function of temperature at a constant height above the sample, we can accurately extract relative changes in $\lambda(T)$, even in the presence of uncertainties in the geometric factors. To determine the temperature dependence of $\lambda$, we measure $M$ at a fixed position as a function of temperature, while maintaining light mechanical contact with the sample. Assuming that $M$ measured at 50 mK reasonably approximates $\lambda_0 = \lambda(T = 0)$ at a given position, we can obtain $\lambda(T)/\lambda_0 - 1 = \delta\lambda(T)\lambda_0$ from $\frac{M(z_o,T)}{M(z_o,T=0)} = \frac{\lambda_0^2}{\lambda^2(T)}$.

Figure 2(a) shows an image of the local magnetic response acquired by scanning several microns above the sample surface while maintaining the sample temperature at 20 mK. The image reveals micrometer-scale variations in the local magnetic susceptibility, and accordingly $\lambda$. Next, we conduct detailed temperature-dependent measurements of the penetration depth at two positions on the sample surface marked in Fig. 2(a). In Fig. 2(b), we show $\delta\lambda(T)/\lambda_0$ versus temperature for these two positions. We find a stronger diamagnetic response at base temperature and a higher local critical temperature, $T_c$, at position 1 than at position 2. For both positions, we observe no significant difference between data collected upon warming and cooling indicating that we sweep temperature sufficiently slow for the sample to thermalize.

In Fig. 2(c), we plot $\delta\lambda(T)/\lambda_0$ as a function of $T^2/T_c^2$ for both positions. The data fall on a straight line, indicating that for $T < 0.4T_c$, $\lambda(T)$ exhibits a $T^2$ temperature dependence.

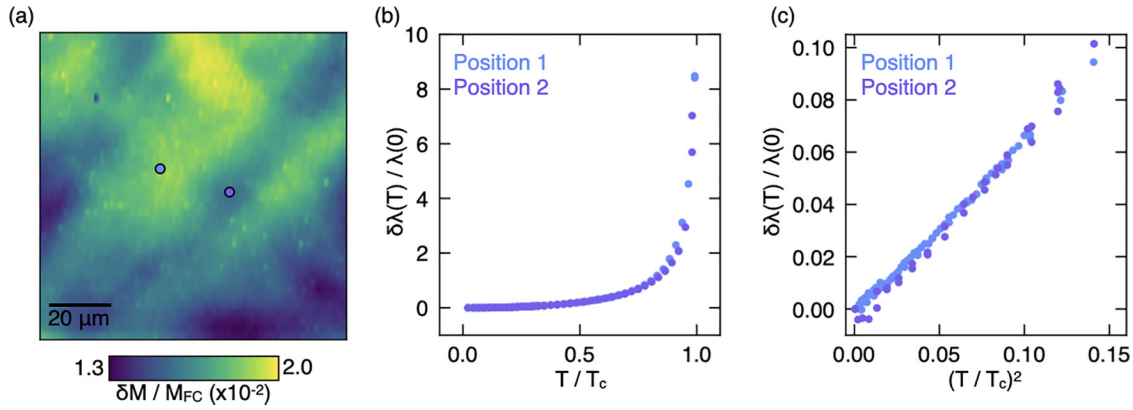


FIG. 2. (a) Spatial map at 20 mK of the local diamagnetic response. The two dots indicate the locations where detailed temperature-dependent data were acquired. The leftmost dot (blue) had a higher local superconducting transition temperature $T_c = 0.90$ K than the right dot (purple), with $T_c = 0.85$ K. (b) $\delta\lambda(T) = \lambda(T) - \lambda(0)$, normalized by $\lambda(0)$ at the positions indicated in (a). (c) $\delta\lambda(T)/\lambda(0)$ plotted against $(T/T_c)^2$.

A temperature dependence of $\lambda(T) \sim T^2$ has been observed previously in high-quality single crystals of $Sr_2RuO_4$ using a tunnel diode oscillator technique [19], radio-frequency surface impedance measurements [29], and more recently using scanning SQUID microscopy on single crystals under uniaxial strain [30] and measurements of the upper critical field [27]. The power-law temperature dependence observed in our study and in the single-crystal work provides evidence for nodes in the superconducting gap function of $Sr_2RuO_4$. In the highest purity single crystals, the slope $m$ of the $\delta\lambda(T)/\lambda_0$ vs $(T/T_c)^2$ graph approaches $m \approx 1.0$ [19,27] For our thin-film sample, we find $m \approx 0.6$. The slope of our $\delta\lambda(T)/\lambda_0$ vs $(T/T_c)^2$ plot lies between the slopes of bulk samples with $T_c = 1.2$ K and $T_c = 0.7$ K reported in Ref. [29].

For nodal superconducting order parameters in the clean limit, a linear temperature dependence, $\delta\lambda(T) \sim T$, is expected. In $Sr_2RuO_4$ bulk samples, the $\delta\lambda(T) \sim T^2$ temperature dependence was attributed to nonlocal electrodynamics of the nodal quasiparticles [19,27,30,31]. Impurity scattering can also change the temperature dependence of $\lambda(T)$ for superconductors with nodes in the gap function. For example, for an order parameter with $d_{x^2-y^2}$ symmetry, strong impurity scattering is expected to give $\delta\lambda(T) \sim T^2$ [32]. In our thin-film samples, $T_c \approx 1$ K is suppressed compared to the highest $T_c \approx 1.5$ K observed in bulk samples, which we attribute below to the presence of pair-breaking scattering. Therefore, it is plausible that impurity scattering plays a larger role in determining the superconducting properties of the thin films than in high-purity bulk samples.

To assess whether scattering is sufficient to explain the temperature dependence of the penetration depth in the thin film studied here, we examine the superfluid density across the full temperature range. The normalized superfluid density is directly related to the penetration depth through $\rho_s(T)/\rho_0 = \lambda_0^2/\lambda^2(T)$, where $\rho_0$ is its zero-temperature value. Figure 3 shows the normalized superfluid density for both positions measured in Fig. 2, as well as three additional positions separated by ∼1 mm from the positions shown in Fig. 2. Although we found local variations in both the magnitude of $\rho_s$ and $T_c$, we find that the normalized superfluid density collapses onto a single curve for each position. Additional characterization of the positions shown in Fig. 3 is presented in the Supplemental Material.

In general, the temperature dependence of $\rho_s$ depends among other factors on the gap structure of the superconductor, the underlying band structure, and the scattering in the sample. Nevertheless, it is useful to compare the temperature dependence of $\rho_s$ to expectations from different simplified phenomenological models. In Fig. 3 we directly compare our measurements to calculations of the superfluid density for different superconducting gap functions assuming a single circular Fermi surface in the weak-coupling BCS limit

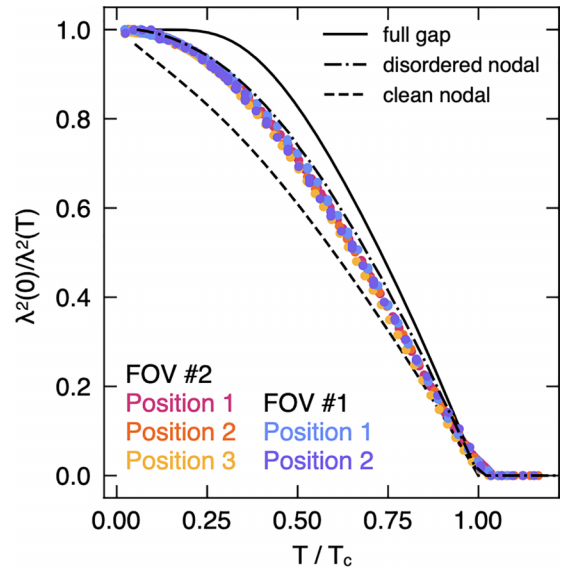


FIG. 3. Normalized superfluid density $\lambda^2(0)/\lambda^2(T)$ measured at the two positions indicated in Fig. 2(a), as well as three additional positions in a second field of view (FOV 2) ∼1 mm away from the field of view shown in Fig. 2. Detailed characterization of FOV 2 is presented in the Supplemental Material. Theoretical curves assuming a weak-coupling BCS superconductor with a single cylindrical Fermi surface are included for comparison.

(see Appendix B for details). We find that neither the fully gapped model nor the $d$-wave models without scattering closely resemble our data.

To include the effect of scattering on the superfluid density, we estimate the strength of pair-breaking scattering in our samples using the theory of Abrikosov and Gor'kov [33]. This theory has been previously used to successfully describe the dependence of $T_c$ on disorder in $Sr_2RuO_4$ bulk samples for defects that were accidentally introduced [14] and for defects that were introduced by substitution [34]. More recently, this theory has been used to capture the change of $T_c$ in thin films in response to defects introduced through high-energy electron irradiation [18]. Within this theory, $T_c$ satisfies

$$\ln\left(\frac{T_{c0}}{T_c}\right) = \Psi\left(\frac{1}{2}+\frac{\Gamma_N}{2\pi T_c}\right) - \Psi\left(\frac{1}{2}\right), \tag{2}$$

where $\Psi$ is the digamma function, $\Gamma_N = \hbar/2\tau k_B$ characterizes the strength of pair-breaking scattering with $\tau$ the corresponding scattering time, $k_B$ the Boltzmann constant, and $\hbar$ the reduced Planck constant, and $T_{c0}$ is the zero-disorder limit of $T_c$. Here we take $T_{c0} = 1.5$ K, the highest value of $T_c$ observed in bulk crystals [27,35]. We observe a suppressed $T_c \approx 0.9$ K in our thin film. This suppression is likely due to pair-breaking scattering, as strain cannot account for the reduction compared to $T_{c0}$. We estimate $\Gamma_N \approx 0.7$ K for our thin film, assuming the same $T_{c0}$ for thin-film and bulk samples.

In bulk samples $T_c$ and $\Gamma_N$ extracted from Eq. (2) correlate strongly with the impurity mean free path determined from the residual resistivity for a given crystal [14,34]. However, this correspondence is absent in thin-film samples, where samples with similar $T_c$ exhibit a wide range of residual resistivity [18], which is why relating $T_c$ to the residual resistivity ratio of our thin film is not possible. This difference in behavior between bulk and thin-film samples is likely due to defects unique to thin films, such as extended out-of-phase boundaries caused by step edges in the substrate due to a slight misorientation between the substrate surface and the (001) LSAT axis [12,16]. These defects increase the residual resistivity but do not strongly suppress $T_c$. In contrast, similarly to bulk samples, the density of point defects such as Ru vacancies have been shown to correlate with $T_c$ in thin films [17,18].

Using the estimated value for $\Gamma_N$, we calculate the normalized superfluid density assuming a $d$-wave gap function with vertical line nodes, a single circular Fermi surface, and including the effects of impurity scattering by following the approach of [36] (details are provided in Appendix B). The result is included as line labeled "disordered nodal" in Fig. 3, and provides much better agreement with our experimental data. We emphasize that this curve is not a fit to the experimental data, but a model for a disordered $d$-wave superconductor with the scattering rate estimated by the experimentally measured $T_c$.

The agreement between this model and the data is remarkable given the simplicity of the Fermi surface and gap structure used in the calculations. Refinement of this model by introducing multiband effects, the experimentally determined Fermi surface, and a realistic pairing potential may improve the agreement between the model and data further.

Despite variations in the local $T_c$, the inferred $\Gamma_N$, and the diamagnetic response at different positions on the sample surface, we find that the normalized superfluid density at each position collapses onto a single curve. In a disordered nodal superconductor with unitary scattering, the shape of the normalized superfluid density curve is independent of $\Gamma_N$ once $\Gamma_N \gtrapprox 0.1T_{c0}$, [36]. Figure S3(c) in the Supplemental Material demonstrates this behavior by showing numerically that the normalized superfluid density collapses onto a single curve for a range of $\Gamma_N$ appropriate for our sample. Qualitative changes in the temperature dependence of the superfluid density are expected only for much smaller values of $\Gamma_N$ [32,36], which we cannot access in the thin-film sample.

The microscopic origin of the local variations in the superfluid density we observe in Fig. 2(a) is not clear. Micron-scale variations in the superconducting properties of high-purity bulk single crystals have also been observed [21,30,37]. Within the impurity scattering model discussed above, variations in the density of scattering sites could be responsible for both the shifts in the local $T_c$ as well as the variation in the low-temperature superfluid density. A quantitative comparison of the observed local changes in superfluid density and $T_c$ with our calculations of the superfluid density above remains inconclusive due to our uncertainty in determining the absolute value of $\lambda$ (see Supplemental Material for details [20], including Refs. [22,38]). Variations in the volume of superconducting $Sr_2RuO_4$ underneath the SQUID could also generate micron-scale changes in the superconducting properties. Natural sources of these changes in the superconducting volume are the inclusion of impurity phases, or variations in the film thickness. However, given the small size of typical impurity inclusions [17], it is not clear whether this mechanism can account for the size of the changes in the diamagnetic response or explain the local variations in the critical temperature.

Nonlocal electrodynamics are predicted to give rise to qualitatively similar penetration depth behavior [31] and have been used to interpret penetration depth measurements on high-quality bulk $Sr_2RuO_4$ samples with critical temperatures close to $T_{c0}$ [19,27,30]. Nonlocal electrodynamics in superconductors is strongly damped by impurity scattering [39,40], and it is unclear whether nonlocal effects can still be detected in thin-film samples with a much higher impurity scattering rate. Yavary *et al.* [40] analyzed the electromagnetic response of a nodal superconductor, incorporating the effects of disorder and nonlocality, and concluded that impurity scattering can obscure the experimental signatures of nonlocal effects. Although our experimental observations are consistent with their findings, a systematic experimental study, similar to Ref. [18], is required to thoroughly investigate the interplay between nonlocal effects and impurity scattering in $Sr_2RuO_4$ thin films.

In summary, we find that the penetration depth in thin-film $Sr_2RuO_4$ shows a $\delta\lambda(T) \propto T^2$ dependence at low temperatures similar to reports in single-crystal bulk samples. This suggests that the gap structure in our thin films is comparable to single-crystal samples and features nodes. Analysis of the full temperature dependence of the superfluid density shows that it can be explained by a nodal superconducting gap combined with scattering in our samples. While this does not exclude nonlocal effects in the Meissner screening, scattering is in our case a sufficient explanation. Future work

investigating changes in $\lambda(T)$ in response to the systematic introduction of disorder, following the approach of [18], may provide a more complete picture of pair-breaking scattering in $Sr_2RuO_4$. Looking forward, our work shows that the delicate superconducting state of $Sr_2RuO_4$ can be preserved in high-quality thin-film samples, which is an important first step toward device-based tests of the order parameter symmetry.

The effect of biaxial strain on the superconducting state in $Sr_2RuO_4$ may also be studied by choosing suitable substrates. Uniaxial strain has proven to be an effective tuning parameter for superconductivity in bulk $Sr_2RuO_4$ [7,8]. Biaxially strained thin-film samples [41] may exhibit a qualitatively different ground state than their uniaxially strained counterparts [42]. The experimental approach demonstrated in this work will provide direct access to new superconducting or magnetic states that emerge in such samples.

## ACKNOWLEDGMENTS

Scanning SQUID measurements were primarily supported through the Cornell Center for Materials Research with funding from the NSF MRSEC program (Grant No. DMR-1719875). Thin-film growth was supported by the National Science Foundation Platform for the Accelerated Realization, Analysis, and Discovery of Interface Materials (PARADIM) under Cooperative Agreement No. DMR-2039380. In addition, this research was funded in part by the Gordon and Betty Moore Foundation's EPiQS Initiative through Grants No. GBMF3850 and No. GBMF9073 to Cornell University. Sample preparation was facilitated in part by the Cornell NanoScale Facility, a member of the National Nanotechnology Coordinated Infrastructure (NNCI), which is supported by the National Science Foundation (Grant No. NNCI-2025233). K.M.S. acknowledges the support of Air Force Office of Scientific Research Grant No. FA9550-21-1-0168 and National Science Foundation Grant No. DMR-2104427.

## APPENDIX A: SCANNING SQUID SUSCEPTOMETRY

Our SQUID susceptometer features a counter-wound field coil pickup loop pair that allows us to null the SQUID response to the field coil excitation. To perform local magnetic susceptibility measurements, the SQUID is retracted as far as possible from the sample surface (about 30 μm) and the susceptometer is balanced by adjusting the current flowing in the two arms of the field coil until the flux coupled into the SQUID pickup loops is minimized. Any remaining SQUID signal after balancing is recorded as an offset signal which represents the response of the SQUID to the field coil in the absence of the sample. This offset is then subtracted from the height sweep data used to characterize the susceptometer geometry in Fig. 1(b) and from all height sweep data used to extract the penetration depth and superfluid density (Figs. 2 and 3). No offset was subtracted from imaging measurements of the local susceptibility [Fig. 2(a)] as these images are used to characterize the spatial variations in the diamagnetic response of the sample.

To avoid spurious signals from vortex motion during the penetration depth measurements, the susceptibility data were collected conducted under near-zero-field conditions. A superconducting solenoid was used to adjust the out-of-plane magnetic field threading the sample until no vortices were observed within the $140\times140\ \mu m^2$ field of view after warming and cooling the sample and SQUID through their respective critical temperatures. This procedure places a rough upper bound of $\frac{\Phi_0}{140\times140\,\mu m^2}\approx 100$ nT on the magnetic flux density in the sample environment. Before and after conducting the temperature sweeps used to acquire the magnetic susceptibility data, the SQUID was used to acquire an image confirming that vortices were absent from the measurement area.

In the main text, we utilized an analytical expression [Eq. (1)] relating the magnetic penetration depth to the geometry of our magnetic susceptibility measurement. Although the data are well fitted by this model, it is strictly only valid in the Pearl limit where $\lambda \gg d$, which applies to our sample. Recent studies on high-quality bulk samples with $T_c$ close to 1.5 K report a low-temperature penetration depth of 120–130 nm [27,28]. Earlier work on bulk samples showed that samples with lower $T_c$ have longer low-temperature penetration depths [29], with estimates λ of 300 and 410 nm for samples with $T_c$ of 1.24 and 0.74 K, respectively. In our thin-film sample, $T_c$ is suppressed compared to the best single crystals similar to the bulk samples in Ref. [29] suggesting $\lambda(T)\gtrsim 10d$ at all measured temperatures. Using calculations of the zero-temperature superfluid density in the presence of disorder, described below, we estimate $\lambda_0$ in our samples ($T_c\approx 900$ mK, $\Gamma_N\approx 0.7$ K) to be about ∼1.7 larger than $\lambda_0$ in the best single crystals, further supporting that $\lambda(T)\gtrsim 10d$ at all temperatures.

Uncertainty in the geometric properties of the susceptometer and sample make a precise determination of the absolute value of λ challenging. Following Ref. [26], we assign a 20% uncertainty to our estimate of the field coil radius $a$, which is based on the lithographic dimensions. We estimate a 20% uncertainty for the film thickness $d$, which is based on the growth rate of the film and the duration of the growth. Based on a 3° uncertainty in the SQUID alignment angle around an initial alignment of ∼10°, we estimate that $z_o$ lies between 3 μm and 5.6 μm. To provide an estimate of the uncertainty in λ given the uncertainties in the geometric parameters of our experiment, we repeated the fitting procedure while varying the geometric parameters within the bounds described above. We found that λ between 210 nm and 860 nm are consistent with the height sweep data shown in Fig. 1 given the geometric uncertainties in our experiment.

To extract the temperature dependence of $\lambda(T)$ from the magnetic susceptibility measurements, we observe that the expression Eq. (1) may be separated into the product of a temperature-dependent part and a temperature-independent part that depends only on the geometric configuration of the SQUID and sample,

$$\frac{M(z,T)}{M_{FC}}=-\frac{ad}{2\lambda^2(T)}\left[1-\frac{2z}{\sqrt{a^2+4z^2}}\right]=\frac{A_{\rm geo}(z)}{\lambda^2(T)}, \quad \text{(A1)}$$

where $A_{\rm geo}(z)=-\frac{ad}{2}(1-\frac{2z}{\sqrt{a^2+4z^2}})$ encodes the sample-susceptometer geometry. From this expression, the temperature dependence of the penetration depth, $\delta\lambda(T)/\lambda_o$, may be

written,

$$\frac{\delta\lambda(T)}{\lambda_o} = \frac{\lambda(T)-\lambda_o}{\lambda_o} = \sqrt{\frac{M(z_o,T=0)}{M(z_o,T)}} - 1, \tag{A2}$$

allowing $\delta\lambda(T)/\lambda_o$ to be directly calculated from measurements of $M(z_o,T)$.

## APPENDIX B: SUPERFLUID DENSITY CALCULATIONS

In this work we calculate the superfluid density in the weak-coupling limit of BCS theory.

To calculate the superfluid density in the presence of disorder, we turn to the self-consistent $t$-matrix approximation [32,36]. Within the approximation, impurities are treated as isotropic point scatters. For simplicity, we again model the system as a single circular Fermi surface, and choose the simplest separable pairing potential $V_{\mathbf{k},\mathbf{k}'}$ with a $d$-wave form factor,

$$V_{\mathbf{k},\mathbf{k}'} = V_0 \Omega_{\mathbf{k}} \Omega_{\mathbf{k}'}, \tag{B1}$$

where

$$\Omega_{\mathbf{k}} \propto \cos k_x a - \cos k_y a, \tag{B2}$$

with $a$ the lattice spacing. Given this Fermi surface and pairing potential, we find solutions to the gap equation,

$$\Delta_{\mathbf{k}} = 2\pi T \sum_{\omega_n>0}^{\omega_0} \left\langle V_{\mathbf{k}\mathbf{k}'} \frac{\Delta_{\mathbf{k}'}}{\left(\tilde{\omega}_n^2 + \Delta_{\mathbf{k}'}^2\right)} \right\rangle_{FS}. \tag{B3}$$

Here, $\Delta_{\mathbf{k}} = \psi(T)\Omega_{\mathbf{k}}$ is the superconducting gap, with $\psi(T)$ the temperature-dependent gap amplitude. $\omega_n = 2\pi T(n+\frac{1}{2})$ are the fermionic Matsubara frequencies and $\langle\cdots\rangle_{FS}$ denotes an average over the Fermi surface. Adding disorder to the system renormalizes the Matsubara frequencies:

$$\tilde{\omega}_n = \omega_n + \pi\Gamma \frac{\langle N_{\mathbf{k}}(\tilde{\omega}_n)\rangle_{FS}}{c^2 + \langle N_{\mathbf{k}}(\tilde{\omega}_n)\rangle_{FS}}, \tag{B4}$$

where $c$ is the cotangent of the scattering phase shift and $\Gamma$ parametrizes the density of scattering sites. The limits $c \ll 1$ and $c \gg 1$ correspond to strong (unitary) and weak (Born) scattering respectively. For bulk samples, impurities on the Ru sites have been shown to act as pair-breaking scatterers $Sr_2RuO_4$ in the strong limit [14,34,43]. In thin films, Ru vacancies have been demonstrated to be the primary form of disorder which limits $T_c$ [17,18,44]. Taking these observations together, we assume that Ru vacancies are also the primary source of disorder in our samples and approximate $c = 0$. Within weak-coupling BCS theory, the gap equation may be solved by finding the $\tilde{\omega}_n$ and $\psi(T)$ that satisfy

$$\ln\left(\frac{T_{c0}}{T}\right) = 2\pi T \sum_{\omega_n>0}^{\infty} \left( \frac{1}{\omega_n} - \left\langle \frac{\Omega_k^2}{\left(\tilde{\omega}_n^2 + \psi^2\Omega_k^2\right)^{1/2}} \right\rangle_{FS} \right). \tag{B5}$$

Equations (B4) and (B5) may be solved self-consistently at a range of temperatures to obtain $\tilde{\omega}_n$ and $\psi(T)$. Once $\tilde{\omega}_n$ and $\psi(T)$ are known, the superfluid density in the presence of disorder may be calculated,

$$\frac{\rho_s(T)}{\rho_{s00}} = 2\pi T \sum_{\omega_n>0}^{\infty} \left\langle \left\langle \frac{\Delta_{\mathbf{k}}^2}{\left(\tilde{\omega}_n^2 + \Delta_{\mathbf{k}}^2\right)^{3/2}} \right\rangle \right\rangle_{FS}. \tag{B6}$$

Here $\langle\langle\cdots\rangle\rangle_{FS}$ denotes a velocity-weighted average over the Fermi surface, and in the case of a circular Fermi surface,

$$\langle\langle A(\phi)\rangle\rangle_{FS} = \frac{\int_0^{2\pi} A(\phi) v_{F,x}^2}{\int_0^{2\pi} v_{F,x}^2}. \tag{B7}$$

Examples of calculated $\psi(T)$ and $\rho_s(T)$ under different impurity scattering strengths $\Gamma_N$ are presented in the Supplemental Material.

## APPENDIX C: SAMPLE GROWTH

The $Sr_2RuO_4$ thin film was grown in a Veeco Gen10 molecular-beam epitaxy (MBE) system on a $(LaAlO_3)_{0.29}$–$(SrAl_{0.5}Ta_{0.5}O_3)_{0.71}$ substrate from CrysTec GmbH. The substrate used for the growth was screened to have a miscut of less than 0.05°, which is important to reduce the formation of out-of-phase boundaries. The films were grown at a substrate temperate of 810 °C as measured using an optical pyrometer operating at 1550 nm. Elemental strontium (99.99% purity) and elemental ruthenium (99.99% purity) evaporated from a low-temperature effusion cell and a Telemark electron-beam evaporator, respectively, were used for growing the $Sr_2RuO_4$ film. The films were grown with a strontium flux of $2.6\times10^{13}$ atoms/(cm$^2$ s) and a ruthenium flux of $1.8\times10^{13}$ atoms/(cm$^2$ s) in a background of distilled ozone ($\sim$ 80% $O_3$ + 20% $O_2$ made from oxygen gas with 99.994% purity). The background oxidant pressure during growth was $3\times10^{-6}$ Torr. At the end of the growth the strontium and ruthenium shutters were closed simultaneously, and the sample was cooled down to below 250 °C in a background pressure of distilled ozone of $3\times10^{-6}$ Torr. Further details of the adsorption-controlled growth conditions for the growth of $Sr_2RuO_4$ thin films by MBE can be found elsewhere [12].


[1] Y. Maeno, H. Hashimoto, K. Yoshida, S. Nishizaki, T. Fujita, J. Bednorz, and F. Lichtenberg, Superconductivity in a layered perovskite without copper, Nature (London) **372**, 532 (1994).

[2] K. Ishida, H. Mukuda, Y. Kitaoka, K. Asayama, Z. Mao, Y. Mori, and Y. Maeno, Spin-triplet superconductivity in $Sr_2RuO_4$ identified by $^{17}$O Knight shift, Nature (London) **396**, 658 (1998).

[3] G. M. Luke, Y. Fudamoto, K. Kojima, M. Larkin, J. Merrin, B. Nachumi, Y. Uemura, Y. Maeno, Z. Mao, Y. Mori *et al.*, Time-reversal symmetry-breaking superconductivity in $Sr_2RuO_4$, Nature (London) **394**, 558 (1998).

[4] K. Nelson, Z. Mao, Y. Maeno, and Y. Liu, Odd-parity superconductivity in $Sr_2RuO_4$, Science **306**, 1151 (2004).

[5] J. Xia, Y. Maeno, P. T. Beyersdorf, M. M. Fejer, and A. Kapitulnik, High resolution polar Kerr effect measurements of

$Sr_2RuO_4$: Evidence for broken time-reversal symmetry in the superconducting state, Phys. Rev. Lett. **97**, 167002 (2006).

[6] F. Kidwingira, J. Strand, D. Van Harlingen, and Y. Maeno, Dynamical superconducting order parameter domains in $Sr_2RuO_4$, Science **314**, 1267 (2006).

[7] C. W. Hicks, D. O. Brodsky, E. A. Yelland, A. S. Gibbs, J. A. Bruin, M. E. Barber, S. D. Edkins, K. Nishimura, S. Yonezawa, Y. Maeno *et al.*, Strong increase of $T_c$ of $Sr_2RuO_4$ under both tensile and compressive strain, Science **344**, 283 (2014).

[8] A. Steppke, L. Zhao, M. E. Barber, T. Scaffidi, F. Jerzembeck, H. Rosner, A. S. Gibbs, Y. Maeno, S. H. Simon, A. P. Mackenzie *et al.*, Strong peak in $T_c$ of $Sr_2RuO_4$ under uniaxial pressure, Science **355**, eaaf9398 (2017).

[9] A. Pustogow, Y. Luo, A. Chronister, Y.-S. Su, D. Sokolov, F. Jerzembeck, A. P. Mackenzie, C. W. Hicks, N. Kikugawa, S. Raghu *et al.*, Constraints on the superconducting order parameter in $Sr_2RuO_4$ from oxygen-17 nuclear magnetic resonance, Nature (London) **574**, 72 (2019).

[10] K. Ishida, M. Manago, K. Kinjo, and Y. Maeno, Reduction of the $^{17}O$ Knight shift in the superconducting state and the heat-up effect by NMR pulses on $Sr_2RuO_4$, J. Phys. Soc. Jpn. **89**, 034712 (2020).

[11] Y.-S. Li, N. Kikugawa, D. A. Sokolov, F. Jerzembeck, A. S. Gibbs, Y. Maeno, C. W. Hicks, J. Schmalian, M. Nicklas, and A. P. Mackenzie, High-sensitivity heat-capacity measurements on $Sr_2RuO_4$ under uniaxial pressure, Proc. Natl. Acad. Sci. USA **118**, e2020492118 (2021).

[12] H. P. Nair, J. P. Ruf, N. J. Schreiber, L. Miao, M. L. Grandon, D. J. Baek, B. H. Goodge, J. P. Ruff, L. F. Kourkoutis, K. M. Shen *et al.*, Demystifying the growth of superconducting $Sr_2RuO_4$ thin films, APL Mater. **6**, 101108 (2018).

[13] C. Tsuei and J. Kirtley, Pairing symmetry in cuprate superconductors, Rev. Mod. Phys. **72**, 969 (2000).

[14] A. P. Mackenzie, R. K. W. Haselwimmer, A. W. Tyler, G. G. Lonzarich, Y. Mori, S. Nishizaki, and Y. Maeno, Extremely strong dependence of superconductivity on disorder in $Sr_2RuO_4$, Phys. Rev. Lett. **80**, 161 (1998).

[15] Z. Q. Mao, Y. Mori, and Y. Maeno, Suppression of superconductivity in $Sr_2RuO_4$ caused by defects, Phys. Rev. B **60**, 610 (1999).

[16] Y. Fang, H. P. Nair, L. Miao, B. Goodge, N. J. Schreiber, J. P. Ruf, L. F. Kourkoutis, K. M. Shen, D. G. Schlom, and B. J. Ramshaw, Quantum oscillations and quasiparticle properties of thin film $Sr_2RuO_4$, Phys. Rev. B **104**, 045152 (2021).

[17] B. H. Goodge, H. P. Nair, D. J. Baek, N. J. Schreiber, L. Miao, J. P. Ruf, E. N. Waite, P. M. Carubia, K. M. Shen, D. G. Schlom *et al.*, Disentangling types of lattice disorder impacting superconductivity in $Sr_2RuO_4$ by quantitative local probes, APL Mater. **10**, 041114 (2022).

[18] J. P. Ruf, H. M. L. Noad, R. Grasset, L. Miao, E. Zhakina, P. H. McGuinness, H. P. Nair, N. J. Schreiber, N. Kikugawa, D. Sokolov, M. Konczykowski, D. G. Schlom, K. M. Shen, and A. P. Mackenzie, Controllable suppression of the unconventional superconductivity in bulk and thin-film $Sr_2RuO_4$ via high-energy electron irradiation, Phys. Rev. Res. **6**, 033178 (2024).

[19] I. Bonalde, B. D. Yanoff, M. Salamon, D. J. Van Harlingen, E. M. E. Chia, Z. Q. Mao, and Y. Maeno, Temperature dependence of the penetration depth in $Sr_2RuO_4$: Evidence for nodes in the gap function, Phys. Rev. Lett. **85**, 4775 (2000).

[20] See Supplemental Material at http://link.aps.org/supplemental/10.1103/PhysRevB.110.144510 for the raw data and additional images, an analysis of the dependence of the superfluid density on the scattering rate, an estimate of the effect of biaxial strain from the substrate on the critical temperature, and resistance and X-ray diffraction measurements on the thin film.

[21] C. A. Watson, A. S. Gibbs, A. P. Mackenzie, C. W. Hicks, and K. A. Moler, Micron-scale measurements of low anisotropic strain response of local $T_c$ in $Sr_2RuO_4$, Phys. Rev. B **98**, 094521 (2018).

[22] F. Jerzembeck, H. S. Røising, A. Steppke, H. Rosner, D. A. Sokolov, N. Kikugawa, T. Scaffidi, S. H. Simon, A. P. Mackenzie, and C. W. Hicks, The superconductivity of $Sr_2RuO_4$ under c-axis uniaxial stress, Nat. Commun. **13**, 4596 (2022).

[23] B. W. Gardner, J. C. Wynn, P. G. Björnsson, E. W. Straver, K. A. Moler, J. R. Kirtley, and M. B. Ketchen, Scanning superconducting quantum interference device susceptometry, Rev. Sci. Instrum. **72**, 2361 (2001).

[24] M. E. Huber, N. C. Koshnick, H. Bluhm, L. J. Archuleta, T. Azua, P. G. Björnsson, B. W. Gardner, S. T. Halloran, E. A. Lucero, and K. A. Moler, Gradiometric micro-SQUID susceptometer for scanning measurements of mesoscopic samples, Rev. Sci. Instrum. **79**, 053704 (2008).

[25] V. Kogan, Meissner response of anisotropic superconductors, Phys. Rev. B **68**, 104511 (2003).

[26] J. R. Kirtley, B. Kalisky, J. A. Bert, C. Bell, M. Kim, Y. Hikita, H. Y. Hwang, J. H. Ngai, Y. Segal, F. J. Walker, C. H. Ahn, and K. A. Moler, Scanning squid susceptometry of a paramagnetic superconductor, Phys. Rev. B **85**, 224518 (2012).

[27] J. F. Landaeta, K. Semeniuk, J. Aretz, K. R. Shirer, D. A. Sokolov, N. Kikugawa, Y. Maeno, I. Bonalde, J. Schmalian, A. P. Mackenzie, and E. Hassinger, Evidence for vertical line nodes in $Sr_2RuO_4$ from nonlocal electrodynamics, Phys. Rev. B **110**, L100503 (2024).

[28] R. Khasanov, A. Ramires, V. Grinenko, I. Shipulin, N. Kikugawa, D. A. Sokolov, J. A. Krieger, T. J. Hicken, Y. Maeno, H. Luetkens, and Z. Guguchia, In-plane magnetic penetration depth in $Sr_2RuO_4$: Muon-spin rotation and relaxation study, Phys. Rev. Lett. **131**, 236001 (2023).

[29] P. J. Baker, R. J. Ormeno, C. E. Gough, Z. Q. Mao, S. Nishizaki, and Y. Maeno, Microwave surface impedance measurements of $Sr_2RuO_4$: The effect of impurities, Phys. Rev. B **80**, 115126 (2009).

[30] E. Mueller, Y. Iguchi, F. Jerzembeck, J. O. Rodriguez, M. Romanelli, E. Abarca-Morales, A. Markou, N. Kikugawa, D. A. Sokolov, G. Oh *et al.*, Superconducting penetration depth through a Van Hove singularity: $Sr_2RuO_4$ under uniaxial stress, Phys. Rev. B **110**, L100502 (2024).

[31] I. Kosztin and A. J. Leggett, Nonlocal effects on the magnetic penetration depth in $d$-wave superconductors, Phys. Rev. Lett. **79**, 135 (1997).

[32] P. J. Hirschfeld and N. Goldenfeld, Effect of strong scattering on the low-temperature penetration depth of a $d$-wave superconductor, Phys. Rev. B **48**, 4219 (1993).

[33] A. A. Abrikosov and L. P. Gor'kov, Contribution to the theory of superconducting alloys with paramagnetic impurities, Zh. Eksp. Teor. Fiz. **39**, 1781 (1960).

[34] N. Kikugawa, A. P. Mackenzie, and Y. Maeno, Effects of in-plane impurity substitution in $Sr_2RuO_4$, J. Phys. Soc. Jpn. **72**, 237 (2003).

[35] T. Akima, S. NishiZaki, and Y. Maeno, Intrinsic superconducting parameters of $Sr_2RuO_4$, J. Phys. Soc. Jpn. **68**, 694 (1999).

[36] N. R. Lee-Hone, J. S. Dodge, and D. M Broun, Disorder and superfluid density in overdoped cuprate superconductors, Phys. Rev. B **96**, 024501 (2017).

[37] E. Mueller, Y. Iguchi, C. Watson, C. W. Hicks, Y. Maeno, and K. A. Moler, Constraints on a split superconducting transition under uniaxial strain in $Sr_2RuO_4$ from scanning squid microscopy, Phys. Rev. B **108**, 144501 (2023).

[38] S. Ghosh, A. Shekhter, F. Jerzembeck, N. Kikugawa, D. A. Sokolov, M. Brando, A. Mackenzie, C. W. Hicks, and B. Ramshaw, Thermodynamic evidence for a two-component superconducting order parameter in $Sr_2RuO_4$, Nat. Phys. **17**, 199 (2021).

[39] M. Tinkham, *Introduction to Superconductivity*, 2nd ed. (Dover Publications, Mineola, NY, 2004).

[40] H. Yavary, Effect of impurity scattering on the low temperature magnetic penetration depth of a nonlocal and nonlinear d-wave superconductor, Phys. C (Amsterdam, Neth.) **450**, 129 (2006).

[41] B. Burganov, C. Adamo, A. Mulder, M. Uchida, P. D. C. King, J. W. Harter, D. E. Shai, A. S. Gibbs, A. P. Mackenzie, R. Uecker, M. Bruetzam, M. R. Beasley, C. J. Fennie, D. G. Schlom, and K. M. Shen, Strain control of fermiology and many-body interactions in two-dimensional ruthenates, Phys. Rev. Lett. **116**, 197003 (2016).

[42] Y.-C. Liu, W.-S. Wang, F.-C. Zhang, and Q.-H. Wang, Superconductivity in $Sr_2RuO_4$ thin films under biaxial strain, Phys. Rev. B **97**, 224522 (2018).

[43] N. Kikugawa, S. Saita, M. Minakata, and Y. Maeno, Effect of Ti substitution on the residual resistivity in the spin-triplet superconductor $Sr_2RuO_4$, Phys. B (Amsterdam, Neth.) **312-313**, 803 (2002).

[44] G. Kim, Y. E. Suyolcu, J. Herrero-Martin, D. Putzky, H. P. Nair, J. P. Ruf, N. J. Schreiber, C. Dietl, G. Christiani, G. Logvenov, M. Minola, P. A. van Aken, K. M. Shen, D. G. Schlom, and B. Keimer, Electronic and vibrational signatures of ruthenium vacancies in $Sr_2RuO_4$ thin films, Phys. Rev. Mater. **3**, 094802 (2019).

# Supplementary Material for "Local magnetic response of superconducting $Sr_2RuO_4$ thin films"

## I. ADDITIONAL MEASUREMENTS OF THE SUPERFLUID DENSITY

In Fig. S1, we provide raw magnetic susceptibility data acquired with the scanning SQUID, used to generate the curves in Fig. 2 of the main text.

To check the consistency of our local measurements of the superfluid density, we compared the results presented in the main text to additional measurements performed in a new field of view on the same sample (Fig. S2). The new field of view was separated by approximately 1 mm from the field of view presented in the main text.

In total, we have performed detailed temperature sweeps at five different locations an the sample surface. We collected these sweeps at locations where the local $T_c$ and $n_s$ where higher than average as well as locations where the local $T_c$ and $n_s$ were lower than surrounding points. Regardless of where we collected our temperature dependent data, we found that the normalized superfluid density to collapse onto a single curve (Fig. S2e).

## II. SENSITIVITY OF THE SUPERFLUID DENSITY ON $\Gamma_N$ AND ANALYSIS OF LOCAL VARIATIONS OF THE SUPERFLUID DENSITY

In the main text, we used the local $T_c$ measured with the scanning SQUID to estimate the value of the impurity scattering rate $\Gamma_N$ in our samples. Using this value of $\Gamma_N$ we found good agreement between a simple model for the superfluid density which includes both nodes in the gap function and disorder. In Fig. S6, we show that the shape of the superfluid density vs. temperature curve resulting from this calculation is not particularly sensitive to the value of $\Gamma_N$ as long as $\Gamma_N \gg 0.1T_{c0}$ where $T_{c0}$ is the critical temperature in the zero disorder case. In particular, for values of $\Gamma_N$ appropriate for our samples, changes in $\Gamma_N$ result in changes in the absolute value of the superfluid density at low temperatures, but do not substantially change the shape of the normalized superfluid density which we plot in Fig. 3 of the main text.

In addition, the model predicts that regions with lower $T_c$ have a lower value of the superfluid density, $\rho$, and correspondingly higher value of $\lambda$ given that $\rho \propto 1/\lambda^2$. We observe this trend in our data in Fig. S1b. Using eq. 1 in the main text we can write $\delta M/M_{FC} = -A_{geo}(z)/\lambda^2$ where $z$ is the height above the sample, and $A_{geo}(z)$ is a temperature-independent geometric factor defined in eq. 1 that is the same for all 5 positions. Fig. S1 shows that the low temperature value of $\delta M/M_{FC}$ is correlated with the local $T_c$, i.e. the temperature at which $\delta M/M_{FC}$ exceeds the noise floor.

In principle, we can take this analysis one step further by comparing the values of $\delta M/M_{FC}$ to the value predicted by the model given the local value of $T_c$. This could help in determining whether the local variations in $T_c$ and the diamagnetic response are due to local variations in the strength of impurity scattering in the sample. In the following, we present this quantitative comparison. We however caution that this analysis is challenging because it requires us to estimate the absolute value of $\lambda_0$ at the different positions. This in turn requires estimating $A_{geo}(z)$, which has large systematic uncertainty. The simple relationship $\delta M/M_{FC} = -A_{geo}(z)/\lambda^2$ noted above is why we focus in the main text on the normalized quantities $\rho/\rho_0$ and $\lambda/\lambda_0$ because we can calculate those directly from our experimental data without knowing the absolute value of $\rho_0$ or $\lambda_0$ ($A_{geo}(z)$ divides out).

The model predicts how $\lambda$ changes as a function $T_c$ and/or $\Gamma_N$. For a quantitative comparison, we need to assume an absolute value of $\lambda_0$ for the zero-disorder case, which we take to be 125 nm based on literature on bulk samples [27]. With this assumption, we can predict $\rho/\rho_{00}$ or equivalently $\lambda/\lambda_{00}$ where $\rho_{00}$ and $\lambda_{00}$ denote the low temperature value in the limit of zero disorder. To compare this with the measured diamagnetic response, we need to estimate the value of $\delta M/M_{FC}$ that would be measured for a film with zero-disorder, i.e., with $\lambda_{00} = 125\,\text{nm}$. This is where $A_{geo}(z)$ becomes important. Using the value of $A_{geo}(z)$ obtained from fitting the height-dependent signal in Fig. 1, evaluated at the height $z_0$ estimated for light mechanical contact, we find poor quantitative agreement between the measured diamagnetic response and the model. If we treat $A_{geo}(z)$ as a free parameter, we find agreement between the predictions of the impurity scattering model and the measured diamagnetic response shown in Fig. S10. This requires a value of $A_{geo}(z)$ that is roughly a factor of 5 smaller than the $A_{geo}(z)$ extracted from the fit in Fig. 1. For example, taking a typical value of $\Gamma_N = 0.37T_{c0}$ (corresponding to $T_c = 0.85\,\text{K}$) for our sample, the impurity scattering model predicts a penetration depth of 205 nm. Quantitative agreement between the diamagnetic response of the sample at the low-temperature and for this value of $\lambda_0$ is obtained for $A_{geo}(z) = 9.2 \times 10^{-16}\,\text{m}^2$, which is smaller than our estimate of $A_{geo}(z) = 5.3\times10^{-15}\,\text{m}^2$ used in Fig. 1, which resulted in an estimate of 480 nm for $\lambda_0$. Refitting the height sweep data in Fig. 1 with this smaller value of $A_{geo}(z)$ returns a best-fit penetration depth of 219 nm, in good agreement with the impurity scattering model.

This comparison remains inconclusive in deciding whether local changes in $T_c$ and the diamagnetic response are originating from local changes in impurity scattering in our sample. Due to the large uncertainty in $A_{geo}(z)$, it is still plausible that spatial variations in the local $T_c$ or $\Gamma_N$ under the SQUID can account for the variations in

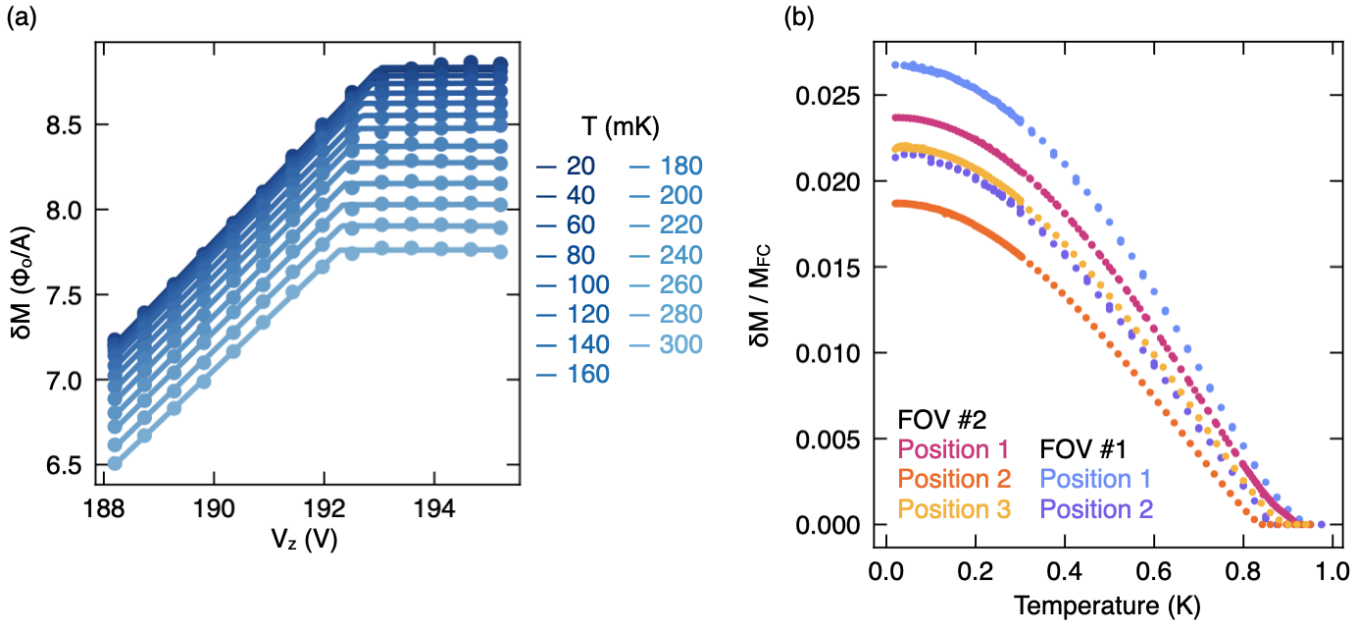


FIG. S1. (a) SQUID-field coil mutual inductance data collected at Position 1 indicated in Figure 2(a) in the main text. As the SQUID is swept towards the sample surface, the strength of the signal detected by the SQUID increases until the SQUID makes mechanical contact with the sample. A piece-wise linear fit to the data is used to extract the value of $V_z$ where the SQUID makes contact as well as $\delta M(z_o, T)$, the change in SQUID-field coil mutual inductance upon mechanical contact with the sample compared to full retraction. As the sample temperature increases, the diamagnetic screening from the sample becomes weaker. (b) Temperature dependence of $\delta M/M_{FC}$ at five different positions on the sample surface. An image of field of view (FOV) 1 is shown in Fig. 2a of the main text and of FOV 2 in Fig. S2. $\delta M(z_o, T)$ is extracted from data by the procedure used in (a) over a wider range of temperatures, and $M_F C$ is the bare mutual inductance between the SQUID pickup loop and field coil. A correlation between the low-temperature value of $\delta M(z_o, T)/M_{FC}$ and the critical temperature is apparent, i.e. curves with a lower temperature onset of diamagnetism saturate to a lower value such that the curves do not intersect.

the diamagnetic screening observed in our sample. However, we cannot rule out that other forms of disorder, as discussed above, also play a role as also discussed in the main text. For accurate measurements of the absolute value of the superfluid density and $\lambda$, a precise calibration of $A_{geo}(z)$ is required.

## III. ESTIMATE OF EPITAXIAL STRAIN INDUCED CHANGES TO $T_c$

A small mismatch in the lattice constants between the LSAT substrate an bulk $Sr_2RuO_4$ generates an epitaxial strain in our thin film samples. At 4 K, the lattice constants of the $Sr_2RuO_4$ thin film are 0.045% larger than in the bulk. In the limit of small strains, changes in $T_c$ generated by epitaxial strain may be estimated from the changes in $T_c$ generated by uniaxial strain along the different crystallographic axes,

$$\Delta T_c = \frac{dT_c}{d\epsilon_a}\epsilon_a + \frac{dT_c}{d\epsilon_b}\epsilon_b + \frac{dT_c}{d\epsilon_c}\epsilon_c, \tag{1}$$

Where $\Delta T_c$ denotes change in $T_c$ due to strain in $Sr_2RuO_4$ grown epitaxially on LSAT. In this case, the LSAT substrate preserves the tetragonal symmetry of $Sr_2RuO_4$, meaning that $\epsilon_a = \epsilon_b$. Due to the symmetry of the crystal structure, we assume $dT_c/d\epsilon_a = dT_c/d\epsilon_b$. Any c-axis strain in our sample is due to Poisson ratio effects, $\epsilon_c = \nu_{ca}(\epsilon_a + \epsilon_b)$, meaning,

$$\Delta T_c = 2\left(\frac{dT_c}{d\epsilon_a} + \nu_{ca}\frac{dT_c}{d\epsilon_c}\right)\epsilon_a, \tag{2}$$

To estimate the parameters in Equation 2, we use measurements of the low-temperature elastic constants [38] and the dependence of $T_c$ on uniaxial stress [21, 22]. In particular, the dependence of $T_c$ on strain, $dT_c/d\epsilon_a$ and $dT_c/d\epsilon_c$ is related to the dependence of $T_c$ on uniaxial stress via the elastic properties of $Sr_2RuO_4$,

$$\frac{dT_c}{d\sigma_a} = \left[(1-\nu_{ab})\frac{dT_c}{d\epsilon_a} + \nu_{ac}\frac{dT_c}{d\epsilon_c}\right]\frac{1}{Y_a} \tag{3}$$

$$\frac{dT_c}{d\sigma_c} = \left[2\nu_{ca}\frac{dT_c}{d\epsilon_a} + \frac{dT_c}{d\epsilon_c}\right]\frac{1}{Y_c}, \tag{4}$$

where $Y_a, Y_c$ are the Young's moduli for a and c axis compression respectively. From uniaxial pressure studies of $T_c$, we find $dT_c/d\sigma_a \approx -78\,\mathrm{mK\,GPa^{-1}}$ [21] and

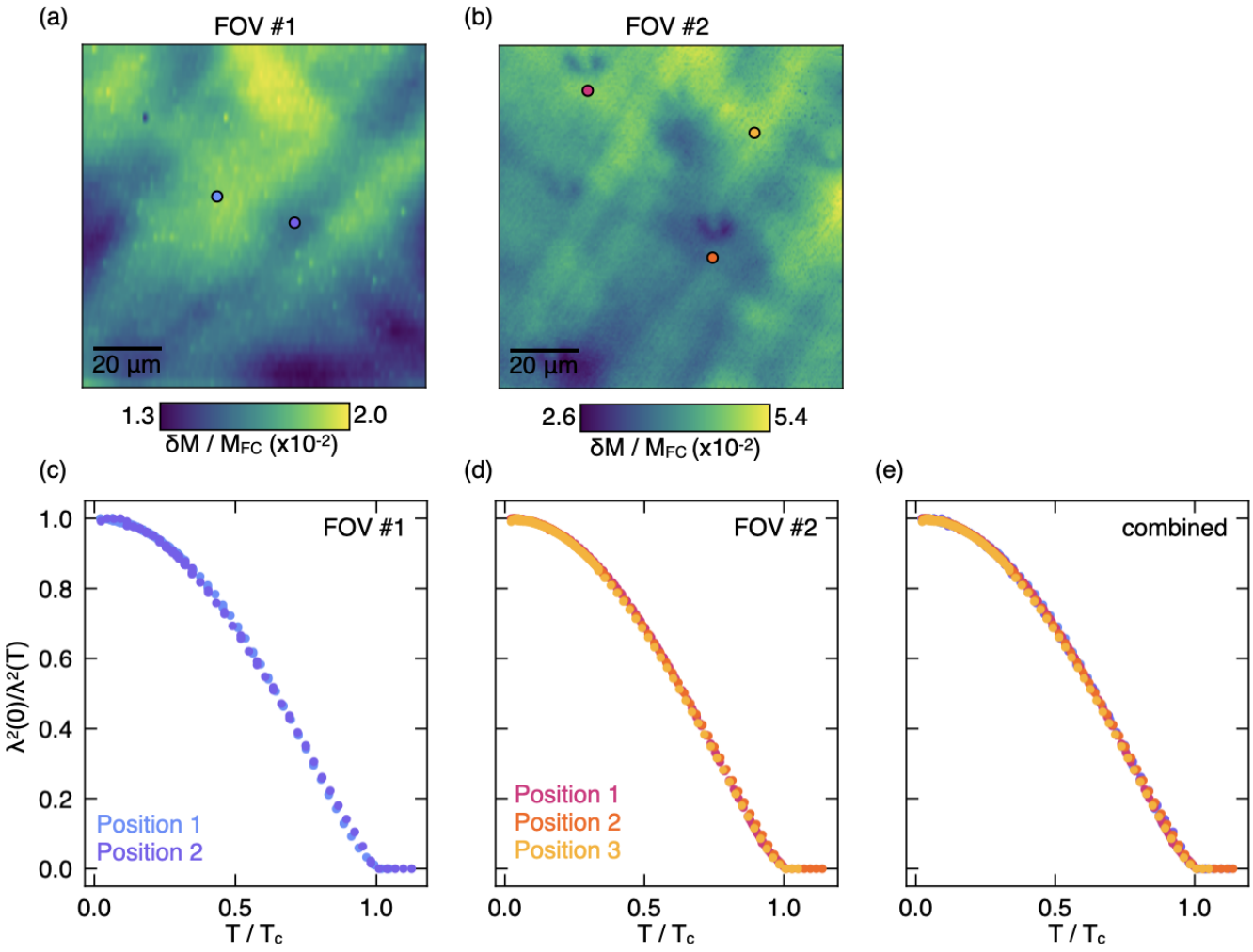


FIG. S2. (a, b) Magnetic susceptibility images of both fields of view where detailed temperature-dependent data were collected. (a) is reproduced from Fig 2. (c) Normalized superfluid density reproduced from Fig 3. (d) Same as (c) except data was collected in FOV 2 at the points indicated in (b). (e) Direct comparison between the superfluid density measured at all five positions.

$dT_c/d\sigma_c \approx -75\,\mathrm{mK\,GPa^{-1}}$ [22]. Combining these values with the elastic properties of $Sr_2RuO_4$ allows us to solve Eqs. 3 and 4 for $dT_c/d\epsilon_a$ and $dT_c/d\epsilon_c$. The values of the Young's moduli and Poisson ratios used for these calculations as well as the dependence of $T_c$ on strain are recorded in Table I. Using these values and Eq. 2, we estimate $\Delta T_c \approx 20\,\mathrm{mK}$

In the discussion above, we have neglected non-linear effects of strain on $Sr_2RuO_4$. In $Sr_2RuO_4$, the dependence of $T_c$ on a-axis strain is predominantly quadratic, with $\Delta T_c \approx A\epsilon_a^2$, and $A \approx 6\,\mathrm{K}/\%^2$ [7, 21]. For our thin-film samples with $\epsilon_a = 0.045\%$, we estimate this contribution to $T_c$ to be $\Delta T_c = 2A\epsilon_a^2 \approx 2\,\mathrm{mK}$, indicating that in our samples strain effects are dominated by the linear dependence of $T_c$ on strain.

TABLE I. $Sr_2RuO_4$ properties used to estimate $\Delta T_c$

| | |
|---|---|
| $dT_c/d\sigma_a$ | $-78\,\mathrm{mK\,GPa^{-1}}$ |
| $dT_c/d\sigma_c$ | $-75\,\mathrm{mK\,GPa^{-1}}$ |
| $Y_a$ | 160 GPa |
| $Y_c$ | 220 GPa |
| $\nu_{ab}$ | 0.51 |
| $\nu_{ac}$ | 0.16 |
| $\nu_{ca}$ | 0.22 |
| $dT_c/d\epsilon_a$ | −22 K |
| $dT_c/d\epsilon_c$ | −7 K |

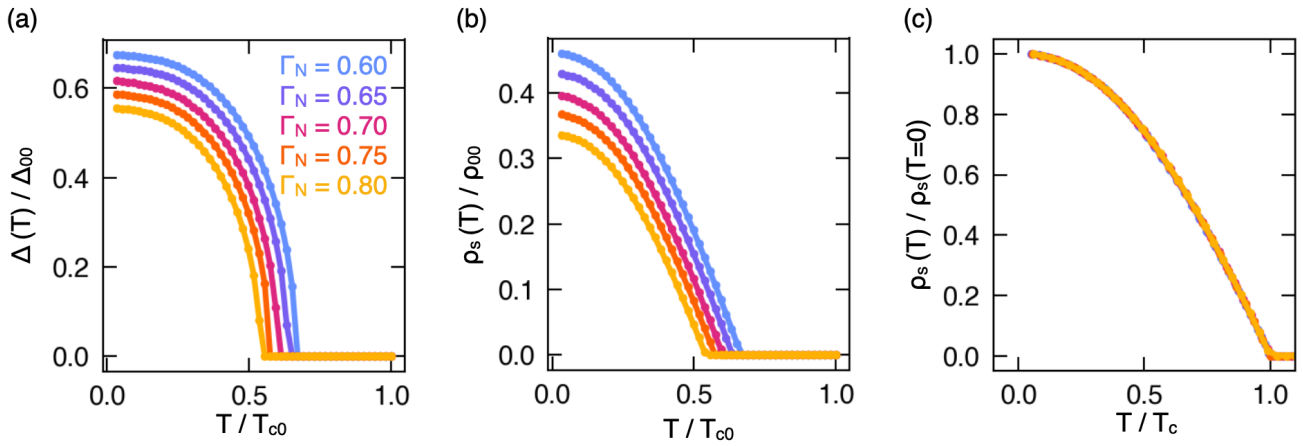


FIG. S3. Dependence of the superfluid density calculations on the scattering rate $\Gamma_N$ for $\Gamma_N \gg 0.1T_{c0}$. (a) Self-consistent gap amplitude calculated as a function of $T$, normalized by the zero temperature, zero disorder gap amplitude $\Delta_{00}$. The calculation is repeated at four representative values of $\Gamma_N$ near the value estimated from the local $T_c$ of the thin film. $\Gamma_N$ in the inset is given in units of $T_{c0}$. (b) Temperature dependent superfluid density calculated using the gap amplitudes in (a), normalized by the zero temperature, zero disorder superfluid density $\rho_{00}$. (c) Normalized superfluid density as a function of temperature calculated in the same way as Fig. 3 in the main text. Each curve is normalized by its own zero temperature value and critical temperature. For the values of $\Gamma_N$ appropriate for our samples, the shape of the curve is insensitive to the exact value of $\Gamma_N$. Only for values of $\Gamma_N < 0.1T_{c0}$, much smaller than those appropriate for our samples, does shape of the superfluid density curve begin to change [32, 36]. For our samples, where $0.6T_{c0} < \Gamma_N < 0.65T_{c0}$ and $\Gamma_N >> 0.1T_{c0}$ for each position measured, the normalized superfluid density is predicted to be independent of the local $T_c$.

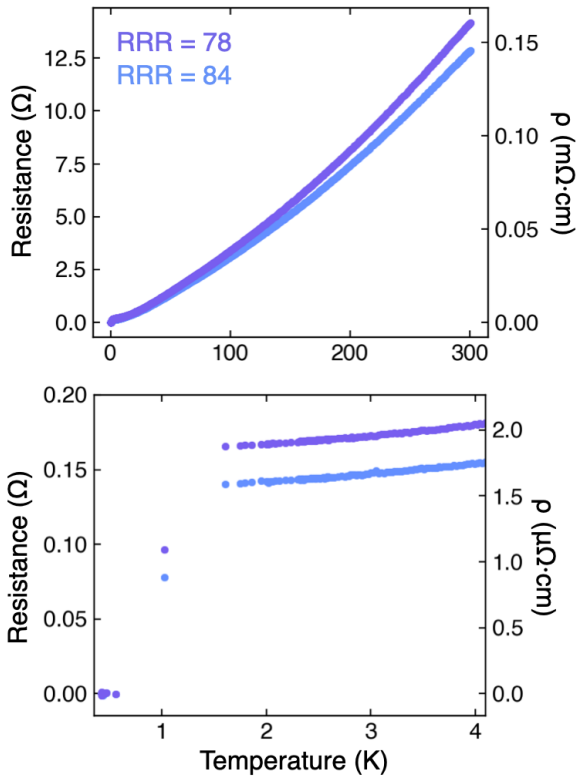


FIG. S4. Temperature dependent resistance for the $Sr_2RuO_4$/LSAT film on which the penetration depth was measured. Top panel shows the full temperature range, bottom panel zooms in on low temperature. Resistance data was recorded in a four-point in-line configuration with the current, $I$, sourced between the outermost contacts and the voltage, $V$, probed between the inner two contacts. The plotted resistance (left axis) is $R = V/I$. Approximately, we estimate the resistivity at 4 K of the film as $\rho = \frac{\pi}{\ln 2} \cdot R \cdot d \approx 1.9\,\mu\Omega\,\mathrm{cm}$ with d the film thickness shown on the right axis. The two measurements (blue/purple) correspond to two different locations on the film. The residual resistivity ratio (RRR), defined as R(T=300 K) / R(T=4 K), is reported in the inset.

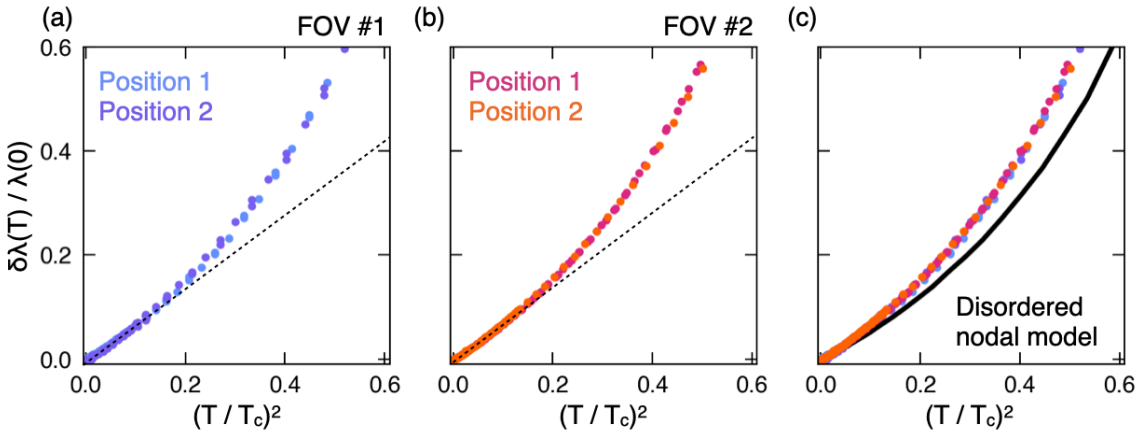


FIG. S5. (a) $\delta\lambda(T)/\lambda(0)$ plotted against $(T/T_c)^2$. Same data as Fig. 2c plotted over a larger range of temperatures. (b) Same as (a) for two different SQUID postions acquired several millimeters away from those shown in (a). (c) Data from (a) and (b), including the $\delta\lambda(T)/\lambda(0)$ calculated from the disordered nodal model for the superfluid density described in the main text. The model collapses to a $T^2$ temperature dependence at the lowest temperatures, but consistently under-estimates the deviation in the penetration depth from $\lambda_0$.

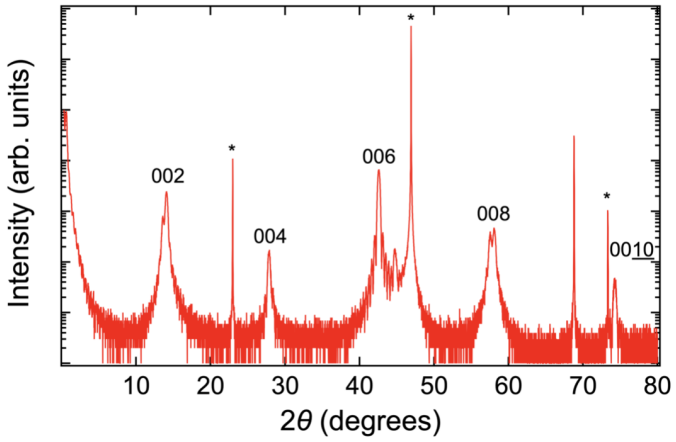


FIG. S6. X-ray diffraction $\theta - 2\theta$ scan of the (001)-oriented $Sr_2RuO_4$ film on which we measured the penetration depth. All of the peaks in the scan can be indexed to either the film or the substrate (asterisks). Slight splitting of the peaks indicates trace inclusions of $Sr_3Ru_2O_7$ intergrowth which cause stacking faults in the film. $Sr_2RuO_4$ thin films with the highest critical temperatures are grown with excess Ru to avoid Ru vacancies. However, this favors the formation of members of the Sr-Ru-O Ruddelson-Popper series with a higher Ru to Sr ratio than $Sr_2RuO_4$.

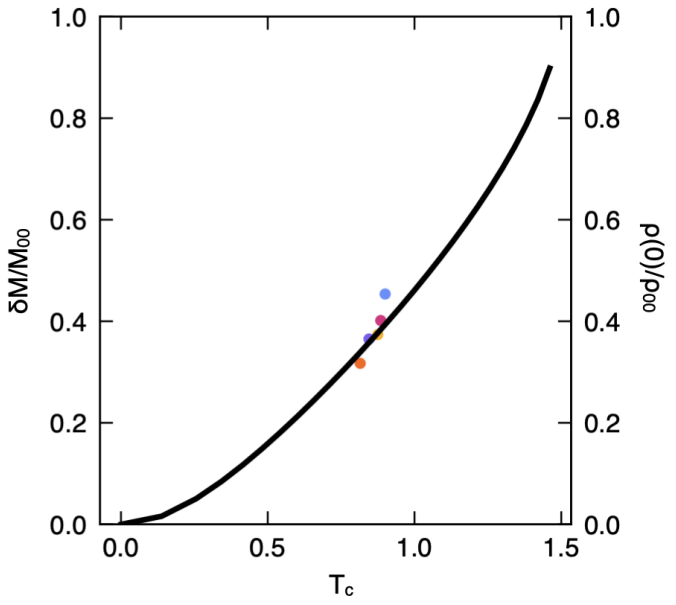


FIG. S7. Calculated superfluid density in the zero-temperature limit, $\rho(0)$, normalized by the zero-temperature, zero-disorder value, $\rho_{00}$, within the impurity scattering model for a nodal superconductor described in the main text (black curve, right axes). The points are the diamagnetic response of the sample in each of the five positions at the lowest temperature measured from Fig. S1 normalized by the response expected in the zero-disorder limit, $M_{00}$, assuming 125 nm for $\lambda_0$ of a disorder free sample. Color of the dots matches the colors of the curves in Fig. S1b. Quantitative agreement between the diamagnetic response and model is obtained by treating the geometric factor $A_{geo}(z)$ as a free parameter instead of estimating it based on the geometry of the experiment(see more details in Sec. III of this supplemental material).

[1] Y. Maeno, H. Hashimoto, K. Yoshida, S. Nishizaki, T. Fujita, J. Bednorz, and F. Lichtenberg, Superconductivity in a layered perovskite without copper, Nature **372**, 532 (1994).

[2] K. Ishida, H. Mukuda, Y. Kitaoka, K. Asayama, Z. Mao, Y. Mori, and Y. Maeno, Spin-triplet superconductivity in $Sr_2RuO_4$ identified by $^{17}O$ Knight shift, Nature **396**, 658 (1998).

[3] G. M. Luke, Y. Fudamoto, K. Kojima, M. Larkin, J. Merrin, B. Nachumi, Y. Uemura, Y. Maeno, Z. Mao, Y. Mori, *et al.*, Time-reversal symmetry-breaking superconductivity in $Sr_2RuO_4$, Nature **394**, 558 (1998).

[4] K. Nelson, Z. Mao, Y. Maeno, and Y. Liu, Odd-parity superconductivity in $Sr_2RuO_4$, Science **306**, 1151 (2004).

[5] J. Xia, Y. Maeno, P. T. Beyersdorf, M. Fejer, and A. Kapitulnik, High resolution polar kerr effect measurements of $Sr_2RuO_4$: Evidence for broken time-reversal symmetry in the superconducting state, Physical Review Letters **97**, 167002 (2006).

[6] F. Kidwingira, J. Strand, D. Van Harlingen, and Y. Maeno, Dynamical superconducting order parameter domains in $Sr_2RuO_4$, Science **314**, 1267 (2006).

[7] C. W. Hicks, D. O. Brodsky, E. A. Yelland, A. S. Gibbs, J. A. Bruin, M. E. Barber, S. D. Edkins, K. Nishimura, S. Yonezawa, Y. Maeno, *et al.*, Strong increase of $T_c$ of $Sr_2RuO_4$ under both tensile and compressive strain, Science **344**, 283 (2014).

[8] A. Steppke, L. Zhao, M. E. Barber, T. Scaffidi, F. Jerzembeck, H. Rosner, A. S. Gibbs, Y. Maeno, S. H. Simon, A. P. Mackenzie, *et al.*, Strong peak in $T_c$ of $Sr_2RuO_4$ under uniaxial pressure, Science **355**, eaaf9398 (2017).

[9] A. Pustogow, Y. Luo, A. Chronister, Y.-S. Su, D. Sokolov, F. Jerzembeck, A. P. Mackenzie, C. W. Hicks, N. Kikugawa, S. Raghu, *et al.*, Constraints on the superconducting order parameter in $Sr_2RuO_4$ from Oxygen-17 nuclear magnetic resonance, Nature **574**, 72 (2019).

[10] K. Ishida, M. Manago, K. Kinjo, and Y. Maeno, Reduction of the $^{17}O$ Knight shift in the superconducting state and the heat-up effect by nmr pulses on $Sr_2RuO_4$, Journal of the Physical Society of Japan **89**, 034712 (2020).

[11] Y.-S. Li, N. Kikugawa, D. A. Sokolov, F. Jerzembeck, A. S. Gibbs, Y. Maeno, C. W. Hicks, J. Schmalian, M. Nicklas, and A. P. Mackenzie, High-sensitivity heat-capacity measurements on $Sr_2RuO_4$ under uniaxial pressure, Proceedings of the National Academy of Sciences **118**, e2020492118 (2021).

[12] H. P. Nair, J. P. Ruf, N. J. Schreiber, L. Miao, M. L. Grandon, D. J. Baek, B. H. Goodge, J. P. Ruff, L. F. Kourkoutis, K. M. Shen, *et al.*, Demystifying the growth of superconducting $Sr_2RuO_4$ thin films, APL Materials **6**, 101108 (2018).

[13] C. Tsuei and J. Kirtley, Pairing symmetry in cuprate superconductors, Reviews of Modern Physics **72**, 969 (2000).

[14] A. Mackenzie, R. Haselwimmer, A. Tyler, G. Lonzarich, Y. Mori, S. Nishizaki, and Y. Maeno, Extremely strong dependence of superconductivity on disorder in $Sr_2RuO_4$, Physical Review Letters **80**, 161 (1998).

[15] Z. Q. Mao, Y. Mori, and Y. Maeno, Suppression of superconductivity in $Sr_2RuO_4$ caused by defects, Physical Review B **60**, 610 (1999).

[16] Y. Fang, H. P. Nair, L. Miao, B. Goodge, N. J. Schreiber, J. P. Ruf, L. F. Kourkoutis, K. M. Shen, D. G. Schlom, and B. J. Ramshaw, Quantum oscillations and quasiparticle properties of thin film $Sr_2RuO_4$, Physical Review B **104**, 045152 (2021).

[17] B. H. Goodge, H. P. Nair, D. J. Baek, N. J. Schreiber, L. Miao, J. P. Ruf, E. N. Waite, P. M. Carubia, K. M. Shen, D. G. Schlom, *et al.*, Disentangling types of lattice disorder impacting superconductivity in $Sr_2RuO_4$ by quantitative local probes, APL Materials **10**, 041114 (2022).

[18] J. P. Ruf, H. M. L. Noad, R. Grasset, L. Miao, E. Zhakina, P. H. McGuinness, H. P. Nair, N. J. Schreiber, N. Kikugawa, D. Sokolov, M. Konczykowski, D. G. Schlom, K. M. Shen, and A. P. Mackenzie, Controllable suppression of the unconventional superconductivity in bulk and thin-film $sr_2ruo_4$ via high-energy electron irradiation, Physical Review Research **6**, 033178 (2024).

[19] I. Bonalde, B. D. Yanoff, M. Salamon, D. Van Harlingen, E. Chia, Z. Mao, and Y. Maeno, Temperature dependence of the penetration depth in $Sr_2RuO_4$: evidence for nodes in the gap function, Physical Review Letters **85**, 4775 (2000).

[20] See Supplemental Material at URL-will-be-inserted-by-publisher .

[21] C. A. Watson, A. S. Gibbs, A. P. Mackenzie, C. W. Hicks, and K. A. Moler, Micron-scale measurements of low anisotropic strain response of local $T_c$ in $Sr_2RuO_4$, Physical Review B **98**, 094521 (2018).

[22] F. Jerzembeck, H. S. Røising, A. Steppke, H. Rosner, D. A. Sokolov, N. Kikugawa, T. Scaffidi, S. H. Simon, A. P. Mackenzie, and C. W. Hicks, The superconductivity of $Sr_2RuO_4$ under c-axis uniaxial stress, Nature Communications **13**, 4596 (2022).

[23] B. W. Gardner, J. C. Wynn, P. G. Björnsson, E. W. Straver, K. A. Moler, J. R. Kirtley, and M. B. Ketchen, Scanning superconducting quantum interference device susceptometry, Review of Scientific Instruments **72**, 2361 (2001).

[24] M. E. Huber, N. C. Koshnick, H. Bluhm, L. J. Archuleta, T. Azua, P. G. Björnsson, B. W. Gardner, S. T. Halloran, E. A. Lucero, and K. A. Moler, Gradiometric micro-SQUID susceptometer for scanning measurements of mesoscopic samples, Review of Scientific Instruments **79**, 053704 (2008).

[25] V. Kogan, Meissner response of anisotropic superconductors, Physical Review B **68**, 104511 (2003).

[26] J. Kirtley, B. Kalisky, J. Bert, C. Bell, M. Kim, Y. Hikita, H. Hwang, J. Ngai, Y. Segal, F. Walker, *et al.*, Scanning squid susceptometry of a paramagnetic superconductor, Physical Review B **85**, 224518 (2012).

[27] J. Landaeta, K. Semeniuk, J. Aretz, K. Shirer, D. Sokolov, N. Kikugawa, Y. Maeno, I. Bonalde, J. Schmalian, A. Mackenzie, *et al.*, Evidence for vertical line nodes in $Sr_2RuO_4$ from nonlocal electrodynamics, arXiv preprint arXiv:2312.05129, to appear in Physical Review B.

[28] R. Khasanov, A. Ramires, V. Grinenko, I. Shipulin, N. Kikugawa, D. A. Sokolov, J. A. Krieger, T. J. Hicken, Y. Maeno, H. Luetkens, and Z. Guguchia, In-plane mag-

netic penetration depth in $Sr_2RuO_4$: Muon-spin rotation and relaxation study, Physical Review Letters **131**, 236001 (2023).

[29] P. J. Baker, R. J. Ormeno, C. E. Gough, Z. Q. Mao, S. Nishizaki, and Y. Maeno, Microwave surface impedance measurements of $Sr_2RuO_4$: The effect of impurities, Physical Review B **80**, 115126 (2009).

[30] E. Mueller, Y. Iguchi, F. Jerzembeck, J. O. Rodriguez, M. Romanelli, E. Abarca-Morales, A. Markou, N. Kikugawa, D. A. Sokolov, G. Oh, *et al.*, Superconducting penetration depth through a van hove singularity: $Sr_2RuO_4$ under uniaxial stress, arXiv preprint arXiv:2312.05130, to appear in Physical Review B.

[31] I. Kosztin and A. J. Leggett, Nonlocal effects on the magnetic penetration depth in d-wave superconductors, Physical Review Letters **79**, 135 (1997).

[32] P. J. Hirschfeld and N. Goldenfeld, Effect of strong scattering on the low-temperature penetration depth of a d-wave superconductor, Physical Review B **48**, 4219 (1993).

[33] A. A. Abrikosov and L. P. Gor'kov, Contribution to the theory of superconducting alloys with paramagnetic impurities, Zhur. Eksptl'. i Teoret. Fiz. **39** (1960).

[34] N. Kikugawa, A. P. Mackenzie, and Y. Maeno, Effects of in-plane impurity substitution in $Sr_2RuO_4$, Journal of the Physical Society of Japan **72**, 237 (2003).

[35] T. Akima, S. NishiZaki, and Y. Maeno, Intrinsic superconducting parameters of $Sr_2RuO_4$, Journal of the Physical Society of Japan **68**, 694 (1999).

[36] N. Lee-Hone, J. Dodge, and D. Broun, Disorder and superfluid density in overdoped cuprate superconductors, Physical Review B **96**, 024501 (2017).

[37] E. Mueller, Y. Iguchi, C. Watson, C. W. Hicks, Y. Maeno, and K. A. Moler, Constraints on a split superconducting transition under uniaxial strain in $Sr_2RuO_4$ from scanning squid microscopy, Physical Review B **108**, 144501 (2023).

[38] S. Ghosh, A. Shekhter, F. Jerzembeck, N. Kikugawa, D. A. Sokolov, M. Brando, A. Mackenzie, C. W. Hicks, and B. Ramshaw, Thermodynamic evidence for a two-component superconducting order parameter in $Sr_2RuO_4$, Nature Physics **17**, 199 (2021).

[39] M. Tinkham, *Introduction to superconductivity* (Dover Publications, 2004).

[40] H. Yavary, Effect of impurity scattering on the low temperature magnetic penetration depth of a nonlocal and nonlinear d-wave superconductor, Physica C: Superconductivity and its applications **450**, 129 (2006).

[41] B. Burganov, C. Adamo, A. Mulder, M. Uchida, P. King, J. Harter, D. Shai, A. Gibbs, A. Mackenzie, R. Uecker, *et al.*, Strain control of fermiology and many-body interactions in two-dimensional ruthenates, Physical Review Letters **116**, 197003 (2016).

[42] Y.-C. Liu, W.-S. Wang, F.-C. Zhang, and Q.-H. Wang, Superconductivity in $Sr_2RuO_4$ thin films under biaxial strain, Physical Review B **97**, 224522 (2018).

[43] N. Kikugawa, S. Saita, M. Minakata, and Y. Maeno, Effect of Ti substitution on the residual resistivity in the spin-triplet superconductor $Sr_2RuO_4$, Physica B: Condensed Matter **312**, 803 (2002).

[44] G. Kim, Y. E. Suyolcu, J. Herrero-Martin, D. Putzky, H. Nair, J. Ruf, N. Schreiber, C. Dietl, G. Christiani, G. Logvenov, *et al.*, Electronic and vibrational signatures of ruthenium vacancies in $Sr_2RuO_4$ thin films, Physical Review Materials **3**, 094802 (2019).